PERGAMON

International Journal of Solids and Structures 40 (2003) 1433–1453

INTERNATIONAL JOURNAL OF SOLIDS and STRUCTURES

www.elsevier.com/locate/ijsolstr

A mixed electric boundary value problem for a two-dimensional piezoelectric crack

Zhenyu Huang [1], Zhen-Bang Kuang *

Department of Engineering Mechanics, Shanghai Jiaotong University, Shanghai, 200240, PR China

Received 13 June 2002; received in revised form 31 October 2002

Abstract

In this paper, a mixed electric boundary value problem for a two-dimensional piezoelectric crack problem is presented, in the sense that the crack face is partly conducting and partly impermeable. By the analytical continuation method, the unknown electric charge distributions on the upper and lower conducting crack faces are reduced to two decoupled singular integral equations and then these two equations are converted into algebraic equations to find the full field solution. Though the results suggest that the stress intensity factors at the crack tip are identical to those of conventional piezoelectric materials, but the electric field and electric displacement are related to the electric boundary conditions on the crack faces. The electric field and electric displacement are singular not only at crack tips but also at the junctures between the impermeable part and conducting parts. Numerical results for the variations of the electric field, electric displacement field and J-integral with respect to the normalized impermeable crack length are shown. Some discussions for the energy release rate and the J-integral are made.

Keywords: Mixed boundary value problem; Piezoelectric ceramic; Fracture; Singular integral equations

1. Introduction

Due to their intrinsic electro-mechanical couplings, piezoelectric ceramics are widely used as sensors, transducers and actuators etc. Defects, such as cracks, dislocations, and voids, inevitably exist during the manufacturing processes or in operation under high applied electro-mechanical loadings. Therefore, the reliability problem emerges and requires a better understanding of the integrity of these materials chosen for engineering devices.

Recently, researches on piezoelectric materials are booming. Although many efforts have been devoted to both of the linear and non-linear analysis of fracture mechanics of piezoelectric materials, the influence of the applied electric field on facture is still not well understood. Parton (1976) first investigated the

* Corresponding author. Fax: +86-21-54743044.
E-mail address: zbkuang@mail.sjtu.edu.cn (Z.-B. Kuang).
[1] Present address: Department of Mechanical and Aerospace Engineering, Princeton University, Princeton, NJ 08544, USA.

0020-7683/02/$ - see front matter © 2002 Elsevier Science Ltd. All rights reserved.
doi:10.1016/S0020-7683(02)00657-1

fracture problem in piezoelectric materials and in his paper the crack was taken to be a permeable slit, i.e. the electric potential and normal component of the electric displacement were continuous across the crack surface. Sosa and Khutoryansky (1996), Gao and Fan (1999) obtained the exact solution of the plane problem for an infinite piezoelectric media with an elliptical cavity under the permeable boundary condition. Based on the solution of Gao and Fan (1999), Huang and Kuang (2000) obtained an asymptotic electro-elastic field near a blunt crack end in a transversely isotropic piezoelectric material, Kuang and Ma (2002) pointed out that for the problem containing a elliptic cavity filled by air can be approximated by an impermeable problem on the elliptic boundary (Appendix C). Deeg (1980), Pak (1990, 1992), addressed the plane and anti-plane fracture problems of piezoelectric materials and obtained a closed form solution of the stress field and electric displacement near the crack tip under the impermeable electric boundary condition. Suo et al. (1992) and Suo (1993) predicted that in the linear frame of piezoelectric theory the electric field always retards the crack propagation for the impermeable electric boundary condition and promotes it under the conducting condition. The mechanical energy release rate (ERR) proposed by Park and Sun (1995) and Jiang and Sun (2001) is used to explain their experiment results, and the results predicted by their theory fit their experimental results well. Gao et al. (1997) and Fulton and Gao (1997) developed a strip electrical saturation model and the local ERR was used to explain the effect of the applied electric field on fracture. Ru (1999a) extended the strip saturation model to study the conducting crack with limited electrical polarization. Zhu and Yang (1997) and Yang and Zhu (1998) investigated the shielding effects by the switch wake of the ferroelectric domain behind the crack. However, none of the developed models can fully explain the effect of the electric field observed in experiments which seems contradicting with each other (Park and Sun, 1995; Wang and Singh, 1997; Fu and Zhang, 1998; Fu and Zhang, 2000).

The mixed boundary value problem can be found in some cases, such as that the electrolyte is not fully filled inside the crack, the distributed internal piece-like separated electrodes in damage detection problem, interdigitated electrodes, thin layer conducting surface becomes discontinuous during fabrication or by electro-mechanical fatigue damage etc. Lynch et al. (1995a,b) and Lynch (1998) found that the electric boundary conditions used in the existing theories are not identical to those of observed in experiments and they stated that whether discharge of the air within the crack happens is crucial in determining the electric field near the crack tip. Breakdown of the dielectric inside the crack was actually observed in their experiments. Zhang et al. (2000, 2001) also pointed out that the local partial electric discharge may make an impermeable crack conduct electrically and change the failure behavior of piezoelectric materials. Recently, Huang and Kuang (2001) conducted an analysis on a non-ideal piezoelectric crack problem using the permeable electric boundary condition. In that model, crack tips are mathematically sharp while in the middle of the crack there is a small gap between the opposing crack faces. They found that there is a very high electric field near the tip within the flaw which may cause the air near the crack tip within the flaw to break down. The discharge process at the gap near the crack tip is a very complex dynamic process. When the electric field obtains a critical value, the air breaks down and becomes conducting gas, but after air breakdown, the electric field diminishes rapidly and the air becomes insulating gas again. In the usual case, this process will be repeated and form discontinuous electric sparks. As a first approximation and qualitatively disscussion, the discharged dielectric within the crack can be modeled by conductors. The electric condition near the crack tip is taken to be conducting, and in the middle of the crack, is taken to be impermeable due to its opening. So, this consideration also leads to a mixed boundary value problem.

In this paper, the mixed electric boundary value problem for a two-dimensional piezoelectric crack is solved. The complex continuation method (Muskhelishvili, 1953) will be employed to solve the full electro-mechanical field. This paper is arranged as follows. In Section 2 we review the basic equations for the generalized piezoelectric plane problem. The derivation of the analytical solutions is elaborated in Section 3. In Section 4, the expressions of the electro-mechanical crack tip field are given and numerical calculations for the variations of the electric field and the electric displacement field with respect to the normalized

impermeable crack length are illustrated. Numerical computation for the J-integral and some discussions on the ERR are presented in Section 5. Finally conclusions are made for the paper.

2. Basic equations

In a fixed rectangular coordinate system (x_1, x_2, x_3), the constitutive equations for linear piezoelectrics of the second kind can be written as

$$\sigma_{ij} = c_{ijkl}u_{k,l} + e_{lij}\phi_{,l}, \quad D_i = e_{ikl}u_{k,l} - \kappa_{il}\phi_{,l} \quad (i,j,k,l = 1,2,3), \tag{1}$$

where repeated Latin indices mean summation and a comma stands for partial differentiation. c_{ijkl} are the elastic stiffnesses under constant electric field, e_{ikl} the piezoelectric stress constants, and κ_{il} the permittivity under constant strain field. $\sigma_{ij}, u_j, D_i, E_i$, and ϕ are stress, displacement, electric displacement, electric field and electric potential respectively. Here we only address the general two-dimensional problem in (x_1, x_2)-plane, i.e. all variables are constant along x_3 axis. (In this paper notations $x_1 = x$ and $x_2 = y$ will be adopted simultaneously.) Following Suo (1993), Chung and Ting (1996) and Kuang and Ma (2002) the generalized displacement solution can be obtained by considering a linear combination of four complex analytical functions,

$$\mathbf{u} = \begin{Bmatrix} u_j \\ \phi \end{Bmatrix} = 2\mathrm{Re}\sum_{\alpha=1}^{4}\mathbf{a}_\alpha f_\alpha(z_\alpha), \quad u_J = 2\mathrm{Re}\sum_{\alpha=1}^{4}a_{J\alpha}f_\alpha(z_\alpha). \tag{2}$$

The uppercase Latin subscript and the Greek subscript all range from 1 to 4, the lowercase Latin subscript from 1 to 3. Note in this paper that implicit summation convention is used only for Latin indices, while for Greek indices we write the summation symbol explicitly. The generalized stress function $\mathbf{\Phi}$ with the components $\Phi_j (j = 1,2,3)$ of the resultant force and the electric displacement flux Φ_4 on an arc, can be represented as,

$$\mathbf{\Phi}(z) = 2\mathrm{Re}\sum_{\alpha=1}^{4}\mathbf{b}_\alpha f_\alpha(z_\alpha), \quad \Phi_J(z) = 2\mathrm{Re}\sum_{\alpha=1}^{4}b_{J\alpha}f_\alpha(z_\alpha), \tag{3}$$

where $z_\alpha = x + p_\alpha y$. The eigenvalues p_α and the eigenvectors $\mathbf{a}_\alpha$ can be obtained from the following equation:

$$\left[\mathbf{Q} + (\mathbf{R} + \mathbf{R}^{\mathrm{T}})p + \mathbf{T}p^2\right]\mathbf{a} = \mathbf{0}, \tag{4}$$

where

$$\mathbf{Q} = \begin{bmatrix} \mathbf{Q}^{\mathrm{E}} & \mathbf{e}_{11} \\ \mathbf{e}_{11}^{\mathrm{T}} & -\kappa_{11} \end{bmatrix}, \quad \mathbf{R} = \begin{bmatrix} \mathbf{R}^{\mathrm{E}} & \mathbf{e}_{21} \\ \mathbf{e}_{21}^{\mathrm{T}} & -\kappa_{12} \end{bmatrix}, \quad \mathbf{T} = \begin{bmatrix} \mathbf{T}^{\mathrm{E}} & \mathbf{e}_{22} \\ \mathbf{e}_{22}^{\mathrm{T}} & -\kappa_{22} \end{bmatrix},$$
$$Q_{ik}^{\mathrm{E}} = c_{i1k1}, \quad R_{ik}^{\mathrm{E}} = c_{i1k2}, \quad T_{ik}^{\mathrm{E}} = c_{i2k2}, \quad (\mathbf{e}_{ij})_s = e_{ijs}, \tag{5}$$

and the eigenvectors $\mathbf{b}_\alpha$ can be obtained from the following relations:

$$\mathbf{b}_\alpha = (\mathbf{R}^{\mathrm{T}} + p_\alpha\mathbf{T})\mathbf{a}_\alpha = -(\mathbf{Q} + p_\alpha\mathbf{R})\mathbf{a}_\alpha/p_\alpha. \tag{6}$$

Let $F_\alpha(z_\alpha) = f'_\alpha(z_\alpha)$, the generalized stresses are as follows:

$$\Sigma_{2J}(z) = \begin{Bmatrix} \sigma_{2j} \\ D_2 \end{Bmatrix} = \Phi_{J,1} = 2\mathrm{Re}\left[\sum_{\alpha=1}^{4}b_{J\alpha}F_\alpha(z_\alpha)\right],$$
$$\Sigma_{1J}(z) = \begin{Bmatrix} \sigma_{1j} \\ D_1 \end{Bmatrix} = -\Phi_{J,2} = -2\mathrm{Re}\left[\sum_{\alpha=1}^{4}b_{J\alpha}p_\alpha F_\alpha(z_\alpha)\right] \tag{7}$$

and the electric fields are

$$E_1 = -u_{4,1} = -2\mathrm{Re}\sum_{\alpha=1}^{4} a_{4\alpha}F_\alpha(z_\alpha),$$
$$E_2 = -u_{4,2} = -2\mathrm{Re}\sum_{\alpha=1}^{4} a_{4\alpha}p_\alpha F_\alpha(z_\alpha). \tag{8}$$

For stable materials eigenvalues cannot be real (Suo et al., 1992; Ting, 1996). The eigenvalues p_α are assumed to be distinctive in this paper.

3. Solutions

Consider a crack of length $2a$ in an infinite piezoelectric material subjected to uniform remote electro-mechanical loadings $\Sigma_{2J}^{\infty}, \Sigma_{1J}^{\infty}$. The crack faces are assumed to be traction-free and there is no external charge on the impermeable part and the electric potential on the conducting crack surfaces is taken to be zero. Let line L_1 and L_3 denote the electrically conducting parts and L_2 denote the impermeable part (see Fig. 1). The length of L_2 is $2b$ and the length of L_1 and L_3 is set to be equal to $\delta = a - b$ for easy analysis.

The electro-mechanical boundary conditions on the crack faces are

$$\sigma_{2j}^{\pm}(x,0) = 0, \quad E_1^{\pm}(x,0) = 0, \quad x \in L_1 \cup L_3, \text{ for the conducting parts,} \tag{9}$$

$$\sigma_{2j}^{\pm}(x,0) = 0, \quad D_2^{\pm}(x,0) = 0, \quad x \in L_2, \text{ for the impermeable part.} \tag{10}$$

The superscripts "+" and "−" represent the value on the upper and lower crack surfaces respectively. The single valued conditions of generalized displacement on the crack faces require

$$\int_L \left[u_{j,x}^{+}(x,0) - u_{j,x}^{-}(x,0)\right]\mathrm{d}x = 0, \quad \int_{L_2} \left[\phi_{,x}^{+}(x,0) - \phi_{,x}^{-}(x,0)\right]\mathrm{d}x = 0, \tag{11}$$

and it is also assumed that there is no extra free charge within the conducting parts, i.e.

$$\int_{L_1} \left[D_y^{+}(x,0) - D_y^{-}(x,0)\right]\mathrm{d}x = 0, \quad \int_{L_3} \left[D_y^{+}(x,0) - D_y^{-}(x,0)\right]\mathrm{d}x = 0. \tag{12}$$

Employing Eqs. (2), (3), (7), (8) and the relation $\overline{F_\alpha^{-}(x)} = \overline{F}_\alpha^{+}(x)$, $\overline{F_\alpha^{+}(x)} = \overline{F}_\alpha^{-}(x)$, Eqs. (9)–(12) can be re-written as

$$\sum_\alpha b_{j\alpha}F_\alpha^{\pm}(x) + \sum_\alpha \bar{b}_{j\alpha}\overline{F}_\alpha^{\mp}(x) = 0, \quad x \in L_1 \cup L_3, \tag{13}$$

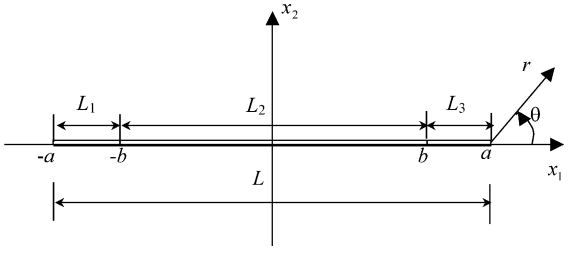

Fig. 1. Crack configuration.

$$\sum_{\alpha} a_{4\alpha}F_{\alpha}^{\pm}(x) + \sum_{\alpha} \bar{a}_{4\alpha}\overline{F}_{\alpha}^{\mp}(x) = 0, \quad x \in L_1 \cup L_3, \tag{14}$$

$$\sum_{\alpha} b_{J\alpha}F_{\alpha}^{\pm}(x) + \sum_{\alpha} \bar{b}_{J\alpha}\overline{F}_{\alpha}^{\mp}(x) = 0, \quad x \in L_2. \tag{15}$$

$$\int_L \sum_{\alpha} \mathrm{Re}\left[a_{j\alpha}\left(F_{\alpha}^{+} - F_{\alpha}^{-}\right)\right]\mathrm{d}x = 0, \tag{16}$$

$$\int_{L_2} \sum_{\alpha} \mathrm{Re}\left[a_{4\alpha}\left(F_{\alpha}^{+} - F_{\alpha}^{-}\right)\right]\mathrm{d}x = 0, \tag{17}$$

$$\int_{L_1} \sum_{\alpha} \mathrm{Re}\left[b_{4\alpha}\left(F_{\alpha}^{+} - F_{\alpha}^{-}\right)\right]\mathrm{d}x = 0, \tag{18}$$

$$\int_{L_3} \sum_{\alpha} \mathrm{Re}\left[b_{4\alpha}\left(F_{\alpha}^{+} - F_{\alpha}^{-}\right)\right]\mathrm{d}x = 0. \tag{19}$$

From the electro-mechanical loading conditions Eqs. (13)–(15) on the crack faces, we have

$$\Sigma_{2J}^{+}(x,0) + \Sigma_{2J}^{-}(x,0) = \sum_{\alpha}\left\lfloor b_{J\alpha}F_{\alpha}^{+}(x) + \bar{b}_{J\alpha}\overline{F}_{\alpha}^{+}(x) + \bar{b}_{J\alpha}\overline{F}_{\alpha}^{-}(x) + b_{J\alpha}F_{\alpha}^{-}(x)\right\rfloor = s_1(x)\delta_{4J}, \tag{20}$$

$$\Sigma_{2J}^{+}(x,0) - \Sigma_{2J}^{-}(x,0) = \sum_{\alpha}\left\lfloor b_{J\alpha}F_{\alpha}^{+}(x) - \bar{b}_{J\alpha}\overline{F}_{\alpha}^{+}(x) + \bar{b}_{J\alpha}\overline{F}_{\alpha}^{-}(x) - b_{J\alpha}F_{\alpha}^{-}(x)\right\rfloor = s_2(x)\delta_{4J}, \tag{21}$$

where

$$s_1(x) = \begin{cases} 0, & x \in L_2 \\ D_2^{+} + D_2^{-}, & x \in L_1 \cup L_3 \end{cases}, \quad s_2(x) = \begin{cases} 0, & x \in L_2 \\ D_2^{+} - D_2^{-}, & x \in L_1 \cup L_3 \end{cases}, \tag{22}$$

which are unknown functions to be determined. Using the analytic continuation method, Eqs. (20) and (21) can be solved as a non-homogenous Riemann–Hilbert problem (Muskhelishvili, 1953). We get

$$\begin{aligned} &\sum_{\alpha}\left\lfloor b_{J\alpha}F_{\alpha}(z) + \bar{b}_{J\alpha}\overline{F}_{\alpha}(z)\right\rfloor = X_a(z)S_{1J}(z) + X_a(z)(\beta_{0J} + \beta_{1J}z), \\ &\sum_{\alpha}\left[b_{J\alpha}F_{\alpha}(z) - \bar{b}_{J\alpha}\overline{F}_{\alpha}(z)\right] = S_{2J}(z) + i\beta_{2J}, \end{aligned} \tag{23}$$

where β_{0J}, β_{1J} and β_{2J} are real numbers and

$$S_{1J}(z) = \frac{1}{2\pi i}\int_L \frac{s_1(t)\delta_{4J}}{(t-z)X_a^{+}(t)}\,\mathrm{d}t, \quad S_{2J}(z) = \frac{1}{2\pi i}\int_L \frac{s_2(t)\delta_{4J}}{t-z}\,\mathrm{d}t, \tag{24}$$

which are analytic on the whole plane except on the crack faces. Note that in the above equations a subscript α for z is dropped and a replacement should be made once the solution for $F_{\alpha}(z)$ obtained. $X_a(z)$ and two other functions $X_b(z)$ and $X_{ab}(z)$ which will appear later are shown as:

$$X_a(z) = \frac{1}{\sqrt{z^2 - a^2}}, \quad X_b(z) = \frac{1}{\sqrt{z^2 - b^2}}, \quad X_{ab}(z) = X_a(z)X_b(z) = \frac{1}{\sqrt{z^2 - a^2}\sqrt{z^2 - b^2}}. \tag{25}$$

The branches of the functions $\sqrt{z^2 - a^2}$ and $\sqrt{z^2 - b^2}$ are taken to be z as z approaches infinity, therefore the values of $X_{ab}(z)$, $X_a(z)$, $X_b(z)$ on the crack upper and lower crack faces are:

$$\begin{cases} X_{ab}^{\pm}(x)=\dfrac{\pm i}{\sqrt{a^2-x^2}\sqrt{x^2-b^2}}, \quad X_b^{+}(x)=X_b^{-}(x)=\dfrac{-1}{\sqrt{x^2-b^2}}, & x\in L_1,\\ X_{ab}^{+}(x)=X_{ab}^{-}(x)=\dfrac{-1}{\sqrt{a^2-x^2}\sqrt{b^2-x^2}}, \quad X_b^{\pm}(x)=\dfrac{\mp i}{\sqrt{b^2-x^2}}, & x\in L_2,\\ X_{ab}^{\pm}(x)=\dfrac{\mp i}{\sqrt{a^2-x^2}\sqrt{x^2-b^2}}, \quad X_b^{+}(x)=X_b^{-}(x)=\dfrac{1}{\sqrt{x^2-b^2}}, & x\in L_3,\\ X_a^{\pm}(x)=\dfrac{\mp i}{\sqrt{a^2-x^2}}, & x\in L. \end{cases} \tag{26}$$

According to the Plemelj formulas (Muskhelishvili, 1953), from Eq. (24), we can get

$$S_{1J}^{+}(x)+S_{1J}^{-}(x)=\frac{1}{\pi i}\int_L \frac{s_1(t)\delta_{4J}}{(t-x)X_a^{+}(t)}\,\mathrm{d}t, \quad S_{1J}^{+}(x)-S_{1J}^{-}(x)=\frac{s_1(x)\delta_{4J}}{X_a^{+}(x)}, \tag{27}$$

$$S_{2J}^{+}(x)+S_{2J}^{-}(x)=\frac{1}{\pi i}\int_L \frac{s_2(t)\delta_{4J}}{t-x}\,\mathrm{d}t, \quad S_{2J}^{+}(x)-S_{2J}^{-}(x)=s_2(x)\delta_{4J}. \tag{28}$$

With Eq. (23) we have

$$F_\alpha(z)=\frac{1}{2}b_{\alpha J}^{-1}[X_a(z)S_{1J}(z)+S_{2J}(z)+X_a(z)(\beta_{0J}+\beta_{1J}z)+i\beta_{2J}], \tag{29}$$

where $b_{\alpha J}^{-1}$ is the element of $[b_{J\alpha}]^{-1}$. Recalling the remote loading condition, we have

$$\begin{cases} \Sigma_{2J}^{\infty}=2\mathrm{Re}\Big[\sum_{\alpha=1}^{4} b_{J\alpha}F_\alpha(\infty)\Big]=\mathrm{Re}[\beta_{1J}+i\beta_{2J}]=\beta_{1J}\\ \Sigma_{1J}^{\infty}=-2\mathrm{Re}\Big[\sum_{\alpha=1}^{4} b_{J\alpha}p_\alpha F_\alpha(\infty)\Big]=-\mathrm{Re}\Big[\sum_{\alpha=1}^{4} b_{J\alpha}p_\alpha b_{\alpha K}^{-1}(\beta_{1K}+i\beta_{2K})\Big] \end{cases} \tag{30}$$

so the unknown constants β_{1J}, β_{2J} can be obtained (Huang and Kuang, 2001). With Eq. (29), one arrives at:

$$\begin{aligned} F_\alpha^{+}(x)+F_\alpha^{-}(x)&=\frac{1}{2}b_{\alpha J}^{-1}\big[X_a^{+}(x)\big(S_{1J}^{+}(x)-S_{1J}^{-}(x)\big)+S_{2J}^{+}(x)+S_{2J}^{-}(x)+2i\beta_{2J}\big],\\ F_\alpha^{+}(x)-F_\alpha^{-}(x)&=\frac{1}{2}b_{\alpha J}^{-1}\big[X_a^{+}(x)\big(S_{1J}^{+}(x)+S_{1J}^{-}(x)\big)+S_{2J}^{+}(x)-S_{2J}^{-}(x)+2X_a^{+}(x)(\beta_{0J}+\beta_{1J}x)\big]. \end{aligned} \tag{31}$$

After an algebraic manipulation for Eq. (14), we have

$$\mathrm{Re}\sum_\alpha \lfloor a_{4\alpha}\big(F_\alpha^{+}(x)+F_\alpha^{-}(x)\big)\rfloor=0, \quad x\in L_1\cup L_3, \tag{32}$$

$$\mathrm{Re}\sum_\alpha \lfloor a_{4\alpha}\big(F_\alpha^{+}(x)-F_\alpha^{-}(x)\big)\rfloor=0, \quad x\in L_1\cup L_3. \tag{33}$$

According to Suo et al. (1992), define $Y_{IJ}=\sum_\alpha i a_{I\alpha}b_{\alpha J}^{-1}$ and $H_{IJ}=Y_{IJ}+\overline{Y}_{IJ}$, the former is a Hermite matrix and the latter a real symmetric matrix. The dimensions of Y_{IJ} can be found in Suo et al. (1992). We have

$$\begin{aligned} \sum_\alpha \mathrm{Re}\lfloor a_{J\alpha}\big(F_\alpha^{+}\pm F_\alpha^{-}\big)\rfloor&=\sum_\alpha\sum_\beta \mathrm{Re}\Big\lfloor a_{J\alpha}b_{\alpha K}^{-1}b_{K\beta}\Big(F_\beta^{+}\pm F_\beta^{-}\Big)\Big\rfloor\\ &=\sum_\alpha\sum_\beta \mathrm{Im}\Big[i a_{J\alpha}b_{\alpha K}^{-1}b_{K\beta}\Big(F_\beta^{+}\pm F_\beta^{-}\Big)\Big]=\sum_\alpha \mathrm{Im}\big[Y_{JK}b_{K\alpha}\big(F_\alpha^{+}\pm F_\alpha^{-}\big)\big] \end{aligned} \tag{34}$$

With Eqs. (31)–(33), one reaches

$$\mathrm{Im}\big\{Y_{4J}\lfloor X_a^{+}(x)(S_{1J}^{+}(x)-S_{1J}^{-}(x))+S_{2J}^{+}(x)+S_{2J}^{-}(x)+2i\beta_{2J}\rfloor\big\}=0, \quad x\in L_1\cup L_3, \tag{35}$$

$$\mathrm{Im}\left\{Y_{4J}\left\lfloor X_a^+(x)(S_{1J}^+(x)+S_{1J}^-(x))+S_{2J}^+(x)-S_{2J}^-(x)+2X_a^+(x)(\beta_{0J}+\beta_{1J}x)\right\rfloor\right\}=0,\quad x\in L_1\cup L_3. \tag{36}$$

Invoking Eqs. (27) and (28), it is not difficult to show that

$$\mathrm{Im}\left\{Y_{44}\left[s_1(x)+\frac{1}{\pi i}\int_L\frac{s_2(t)}{t-x}\,\mathrm{d}t\right]+2iY_{4J}\beta_{2J}\right\}=0,\quad x\in L_1\cup L_3. \tag{37}$$

$$\mathrm{Im}\left\{Y_{44}X_a^+(x)\frac{1}{\pi i}\int_L\frac{s_1(t)}{(t-x)X_a^+(t)}\,\mathrm{d}t+2Y_{4J}X_a^+(x)(\beta_{0J}+\beta_{1J}x)\right\}=0,\quad x\in L_1\cup L_3. \tag{38}$$

Ru (1999b) showed that

$$Y_{44}-\overline{Y}_{44}=0\quad\text{or}\quad \mathrm{Im}[Y_{44}]=0. \tag{39}$$

Hence the integral equations (37) and (38) for the unknown functions $s_1(x)$ and $s_2(x)$ are decoupled,

$$\frac{H_{44}}{\pi i}\int_L\frac{s_2(t)}{t-x}\,\mathrm{d}t+2iH_{4J}\beta_{2J}=0,\quad x\in L_1\cup L_3. \tag{40}$$

$$H_{44}\frac{1}{\pi i}\int_L\frac{s_1(t)}{(t-x)X_a^+(t)}\,\mathrm{d}t+2H_{4J}(\beta_{0J}+\beta_{1J}x)=0,\quad x\in L_1\cup L_3. \tag{41}$$

It is supposed that the electric displacement has the following structure:

$$D_2(z)=\mathrm{Re}[P_{ab}(z)X_{ab}(z)+P_a(z)X_a(z)+P_b(z)X_b(z)]+C, \tag{42}$$

where polynomials $P_{ab}(z)$, $P_a(z)$, $P_b(z)$ are of the order of z^2, z and z respectively and C is a real constant. So from Eqs. (42), (22), (26), we get

$$\begin{cases}s_2(x)=2i(\gamma_0+\gamma_1x+\gamma_2x^2)X_{ab}^+(x)+2i(\gamma_3+\gamma_4x)X_a^+(x)\\ s_1(x)=2(\gamma_5+\gamma_6x)X_b^+(x)+2C\end{cases}\quad x\in L_1\cup L_3, \tag{43}$$

where γ_i, $i=0$–6 are real constants. Substituting the expressions of $s_1(x)$, $s_2(x)$ into the singular integral equations (40) and (41), we get

$$\frac{H_{44}}{\pi i}\int_{L_1\cup L_3}\frac{(\gamma_0+\gamma_1t+\gamma_2t^2)X_{ab}^+(t)+(\gamma_3+\gamma_4t)X_a^+(t)}{t-x}\,\mathrm{d}t+H_{4J}\beta_{2J}=0,\quad x\in L_1\cup L_3, \tag{44}$$

$$H_{44}\frac{1}{\pi i}\int_{L_1\cup L_3}\frac{2(\gamma_5+\gamma_6t)X_b^+(t)+2C}{(t-x)X_a^+(t)}\,\mathrm{d}t+2H_{4J}(\beta_{0J}+\beta_{1J}x)=0,\quad x\in L_1\cup L_3. \tag{45}$$

Now the solutions for the integral equations are reduced to find the seven unknown constants γ_i, $i=0$–6. Using the singular integrals listed in Appendix A, we have

$$\begin{cases}\dfrac{H_{44}}{\pi i}\left[-\pi i\gamma_2+\displaystyle\int_{L_1\cup L_3}\frac{(\gamma_3+\gamma_4t)X_a^+(t)}{t-x}\,\mathrm{d}t\right]+H_{4J}\beta_{2J}=0\\ H_{44}\dfrac{1}{\pi i}2(-\pi i\gamma_5-\pi i\gamma_6x)+H_{44}\dfrac{1}{\pi i}\displaystyle\int_{L_1\cup L_3}\frac{2C}{(t-x)X_a^+(t)}\,\mathrm{d}t+2H_{4J}(\beta_{0J}+\beta_{1J}x)=0\end{cases},\quad x\in L_1\cup L_3. \tag{46}$$

In Eq. (46) the integral terms are kept since their closed forms are very complicated. The above polynomials must hold for all x, therefore we have

$$C=0,\quad \gamma_3=\gamma_4=0,\quad \gamma_2=H_{4J}\beta_{2J}/H_{44},\quad \gamma_5=H_{4J}\beta_{0J}/H_{44},\quad \gamma_6=H_{4J}\beta_{1J}/H_{44}. \tag{47}$$

Using Eqs. (22), (24), (26)–(28) and integrals in Appendix A, the second term of Eq. (31) can be reduced to

$$F_\alpha^+(x)-F_\alpha^-(x)=\begin{cases} b_{\alpha J}^{-1}X_a^+(x)\big[-\delta_{4J}(\gamma_5+\gamma_6x)+i\delta_{4J}(\gamma_0+\gamma_1x+\gamma_2x^2)X_b^+(x)+(\beta_{0J}+\beta_{1J}x)\big], & x\in L_1\cup L_3\\ b_{\alpha J}^{-1}X_a^+(x)\left[\delta_{4J}(\gamma_5+\gamma_6x)\left(\frac{X_b^+(x)}{X_a^+(x)}-1\right)+(\beta_{0J}+\beta_{1J}x)\right], & x\in L_2\end{cases} \tag{48}$$

therefore,

$$\sum_\alpha b_{J\alpha}(F_\alpha^+-F_\alpha^-)=X_a^+(x)\big[-\delta_{4J}(\gamma_5+\gamma_6x)+i\delta_{4J}(\gamma_0+\gamma_1x+\gamma_2x^2)X_b^+(x)+(\beta_{0J}+\beta_{1J}x)\big],\quad x\in L_1\cup L_3 \tag{49}$$

and

$$\sum_\alpha b_{J\alpha}(F_\alpha^+-F_\alpha^-)=X_a^+(x)\left[\delta_{4J}(\gamma_5+\gamma_6x)\left(\frac{X_b^+(x)}{X_a^+(x)}-1\right)+(\beta_{0J}+\beta_{1J}x)\right],\quad x\in L_2. \tag{50}$$

From Eq. (49) there is

$$\mathrm{Re}\sum_\alpha b_{4\alpha}(F_\alpha^+-F_\alpha^-)=\mathrm{Re}\big\lfloor i\big(\gamma_0+\gamma_1x+\gamma_2x^2\big)X_b^+(x)X_a^+(x)\big\rfloor,\quad x_1\in L_1\cup L_3$$

So, substituting above equation into Eqs. (18) and (19) which represent that there is no extra free charge on the conducting surface parts, we get

$$\int_{-a}^{-b}\frac{\gamma_0+\gamma_1x+\gamma_2x^2}{\sqrt{a^2-x^2}\sqrt{b^2-x^2}}\,\mathrm{d}x=0,\quad \int_b^a\frac{\gamma_0+\gamma_1x+\gamma_2x^2}{\sqrt{a^2-x^2}\sqrt{b^2-x^2}}\,\mathrm{d}x=0. \tag{51}$$

The above equations give the solutions for γ_0, γ_1, γ_2 as

$$\gamma_1=0,\quad \gamma_0=-\gamma_2I_2/I_1, \tag{52}$$

where

$$I_2=\int_b^a\frac{x^2}{\sqrt{x^2-b^2}\sqrt{a^2-x^2}}\,\mathrm{d}x,\quad I_1=\int_b^a\frac{1}{\sqrt{x^2-b^2}\sqrt{a^2-x^2}}\,\mathrm{d}x, \tag{53}$$

which are two elliptic integrals and their values can be obtained by numerical integration program or by looking up the Table of elliptic integral (Gradshteyn and Ryzhik, 1980). With Eqs. (34), (49), (50), we have

$$\begin{aligned}\sum_\alpha\mathrm{Re}\lfloor a_{J\alpha}(F_\alpha^+-F_\alpha^-)\rfloor&=\mathrm{Im}\big\{X_a^+(x)\big[-Y_{J4}(\gamma_5+\gamma_6x)+iY_{J4}(\gamma_0+\gamma_2x^2)X_b^+(x)+Y_{JK}(\beta_{0K}+\beta_{1K}x)\big]\big\}\\&=X_a^+(x)\big[-H_{J4}(\gamma_5+\gamma_6x)+i(Y_{J4}-\overline{Y}_{J4})(\gamma_0+\gamma_2x^2)X_b^+(x)\\&\quad+H_{JK}(\beta_{0K}+\beta_{1K}x)\big]/2i,\quad x\in L_1\cup L_3,\end{aligned} \tag{54}$$

and

$$\begin{aligned}\sum_\alpha\mathrm{Re}\lfloor a_{J\alpha}(F_\alpha^+-F_\alpha^-)\rfloor&=\mathrm{Im}\left\{X_a^+(x)\left[Y_{J4}(\gamma_5+\gamma_6x)\left(\frac{X_b^+(x)}{X_a^+(x)}-1\right)+Y_{JK}(\beta_{0K}+\beta_{1K}x)\right]\right\}\\&=X_a^+(x)\left[H_{J4}(\gamma_5+\gamma_6x)\left(\frac{X_b^+(x)}{X_a^+(x)}-1\right)+H_{JK}(\beta_{0K}+\beta_{1K}x)\right]\Big/2i,\quad x\in L_2.\end{aligned} \tag{55}$$

Hence, from Eq. (17), which represents the single valued condition of electric potential on the impermeable surface part, one has

$$\int_{L_2} X_a^+(x)\left[H_{44}(\gamma_5+\gamma_6 x)\left(\frac{X_b^+(x)}{X_a^+(x)}-1\right)+H_{4K}(\beta_{0K}+\beta_{1K}x)\right]\mathrm{d}x=0. \tag{56}$$

In the above equation, the integral containing the odd function $xX_a^+(x)$ is identically equal to zero, so the condition is equivalent to

$$\int_{L_2}\left[H_{44}\gamma_5(X_b^+(x)-X_a^+(x))+X_a^+(x)H_{4K}\beta_{0K}\right]\mathrm{d}x=0. \tag{57}$$

Invoking the relation $\gamma_5=H_{4J}\beta_{0J}/H_{44}$ in Eq. (47), we get

$$\int_{L_2} H_{44}\gamma_5 X_b^+(x)\,\mathrm{d}x=0. \tag{58}$$

Hence we have

$$\gamma_5=H_{4K}\beta_{0K}/H_{44}=0. \tag{59}$$

Using Eqs. (49) and (50), the displacement single valued condition Eq. (16) is rewritten as

$$\begin{aligned}&\int_{L_1\cup L_3} X_a^+(x)\left[-H_{j4}(\gamma_5+\gamma_6 x)+i(Y_{j4}-\overline{Y}_{j4})(\gamma_0+\gamma_2x^2)X_b^+(x)+H_{jK}(\beta_{0K}+\beta_{1K}x)\right]\mathrm{d}x\\&\quad+\int_{L_2} X_a^+(x)\left[-H_{j4}(\gamma_5+\gamma_6 x)+H_{jK}(\beta_{0K}+\beta_{1K}x)\right]\mathrm{d}x=0.\end{aligned} \tag{60}$$

With Eq. (52), it is known that

$$\int_{L_1\cup L_3} X_a^+(x)(\gamma_0+\gamma_2x^2)X_b^+(x)\,\mathrm{d}x=0.$$

So Eq. (60) can be further simplified to be

$$\begin{aligned}&\int_{L_1\cup L_3} X_a^+(x)\left[-H_{j4}\gamma_6 x+H_{jK}(\beta_{0K}+\beta_{1K}x)\right]\mathrm{d}x+\int_{L_2} X_a^+(x)\left[-H_{j4}\gamma_6 x+H_{jK}(\beta_{0K}+\beta_{1K}x)\right]\mathrm{d}x\\&\quad=H_{jK}\beta_{0K}\int_{L_1\cup L_3} X_a^+(x)\,\mathrm{d}x+H_{jK}\beta_{0K}\int_{L_2} X_a^+(x)\,\mathrm{d}x=H_{jK}\beta_{0K}\int_{L} X_a^+(x)\,\mathrm{d}x=0.\end{aligned} \tag{61}$$

Hence we have

$$H_{jK}\beta_{0K}=0, \tag{62}$$

together with $\gamma_5=H_{4K}\beta_{0K}/H_{44}=0$ and knowing $\mathbf{H}$ is a non-singular matrix, one arrives at

$$\beta_{0K}=0. \tag{63}$$

Now all the unknown constants are solved. With Eqs. (24) and (43) and the integrals listed in the Appendix A, we have

$$S_{1J}(z)=\frac{\delta_{4J}}{2\pi i}\int_{L_1\cup L_3}\frac{2(\gamma_5+\gamma_6 t)X_b^+(t)}{(t-z)X_a^+(t)}\,\mathrm{d}t=\delta_{4J}\gamma_6 z(X_b(z)/X_a(z)-1), \tag{64}$$

$$S_{2J}(z)=\frac{\delta_{4J}}{2\pi i}\int_{L_1\cup L_3}\frac{2i(\gamma_0+\gamma_1 t+\gamma_2 t^2)X_{ab}^+(t)}{t-z}\,\mathrm{d}t=\delta_{4J}\left[i(\gamma_0+\gamma_2 z^2)X_{ab}(z)-i\gamma_2\right]. \tag{65}$$

Therefore, the field solution Eq. (29) can be written as

$$F_\alpha(z)=\frac{1}{2}b_{\alpha 4}^{-1}\left[\gamma_6 z(X_b(z)-X_a(z))+i(\gamma_0+\gamma_2 z^2)X_{ab}(z)-i\gamma_2\right]+\frac{1}{2}b_{\alpha J}^{-1}[\beta_{1J}zX_a(z)+i\beta_{2J}]. \tag{66}$$

After a substitution of the solution Eq. (66) into Eqs. (7) and (8) and (11) and (12), the boundary conditions are all satisfied. Hence the correctness of Eq. (66) is proved. Let the impermeable length b equal to zero or a, the limit analysis reveals that $\gamma_0=0$ for $b=0$ and $\gamma_0=-a^2\gamma_2$ for $b=a$, so it is not difficult to show that the present solution recovers the conventional impermeable crack and conducting crack solutions.

4. Crack tip fields

In this section, we devote our attention to the near-tip crack tip field. In the following, without losing generality, we only discuss the right crack tip field. As we know, an impermeable crack intensifies an electric field applied perpendicular to the crack, but does not perturb a field parallel to the crack; conversely, a conducting crack intensifies an electric field applied parallel to the crack, but not a field perpendicular to it (Lynch et al., 1995a). The electric displacement intensity factor for the impermeable crack is defined based on $D_2(x,0)$ near the crack tip, but the electric field intensity factor for the conducting crack is on $E_1(x,0)$, so we only give the expressions of $E_1(x,0)$ and $D_2(x,0)$ directly ahead of the crack tip.

Introduce two polar coordinates (r,θ) and (r_b,θ_b) with their origins located at points $(x=a,0)$ and $(x=b,0)$ (where singular fields may be located) respectively. The electro-mechanical field directly ahead of the crack tip on the axis can be obtained after substitution of Eq. (66) into Eqs. (7) and (8)

$$\sigma_{2j}(x)=\frac{\beta_{1j}x}{\sqrt{x^2-a^2}}=\frac{\sigma_{2j}^{\infty}x}{\sqrt{x^2-a^2}}, \tag{67}$$

$$D_2(x)=\frac{H_{4j}\sigma_{2j}^{\infty}x}{H_{44}}\left(\frac{1}{\sqrt{x^2-b^2}}-\frac{1}{\sqrt{x^2-a^2}}\right)+\frac{D_2^{\infty}x}{\sqrt{x^2-b^2}}, \tag{68}$$

$$E_1(x)=\frac{\beta_{2J}H_{4J}(I_2/I_1-x^2)}{2\sqrt{x^2-a^2}\sqrt{x^2-b^2}}-\sigma_{2j}^{\infty}\mathrm{Im}[Y_{4j}]\frac{x}{\sqrt{x^2-a^2}}. \tag{69}$$

From Eq. (67), it is always possible to define stress intensity factors

$$K_{\mathrm{II}}=\sqrt{\pi a}\sigma_{21}^{\infty},\quad K_{\mathrm{I}}=\sqrt{\pi a}\sigma_{22}^{\infty},\quad K_{\mathrm{III}}=\sqrt{\pi a}\sigma_{23}^{\infty}, \tag{70}$$

which is identical to the conventional stress intensity factors for anisotropic materials. However, under the present mixed boundary condition, the near-tip electric field and electric displacement field are complicated. The crack extension is determined by the K-field near the tip, but sometime we also assume that the failure is determined by the maximum tension stress at a distance $x=r_0$ (Kuang, 1982) ahead of the crack tip and this is also valid for a non-ideal crack and two singular points are very near each other. According to this fact, the electric field and electric displacement near the crack tip $x=a$ will be classified into three different cases by the relative magnitude of $\delta=a-b$ and r_0.

Case 1: $\delta\gg r_0$, that is to say the singular field at $x=b$ cannot influence the singular field at the physical crack tip. In this case the electric displacement and electric field intensity factors are identical of those of the conducting crack.

$$K_{\mathrm{D}}=\lim_{r\to 0}\sqrt{2\pi r}D_2(r,0)=-H_{4j}\sigma_{2j}^{\infty}\sqrt{\pi a}/H_{44}, \tag{71}$$

$$K_{\mathrm{E}}=\lim_{r\to 0}\sqrt{2\pi r}E_1(r,0)=\frac{\beta_{2J}H_{4J}\sqrt{\pi}(I_2/I_1-a^2)}{2\sqrt{a}\sqrt{a^2-b^2}}-\sigma_{2j}^{\infty}\sqrt{\pi a}\,\mathrm{Im}[Y_{4j}]. \tag{72}$$

Case 2: $\delta \ll r_0$, which means the point $x = b$ and the point $x = a$ can be treated as one point. Hence the intensity factors are identical to those of the completely impermeable crack.

$$K_{\mathrm{D}} = \lim_{r\to 0} \sqrt{2\pi r} D_2(r, 0,) = D_2^{\infty}\sqrt{\pi a}. \tag{73}$$

$$K_{\mathrm{E}} = \lim_{r\to 0} \sqrt{2\pi r} E_1(r, 0) = -\sqrt{\pi a}\sigma_{2j}^{\infty}\,\mathrm{Im}[Y_{4j}]. \tag{74}$$

Case 3: $\delta \sim r_0$, i.e. the singular field at $x = b$ interacted with the singular field at the physical crack tip but they cannot be treated as one point as in Case 2. In this case, an electric field intensity factor and electric displacement intensity factor (if defined in the same manner as usual) will depend on δ and r. The intensity factors transit from impermeable ones (Case 2) to conducting ones (Case 1) as $\delta/r_0 \ll 1$ shifts to $\delta/r_0 \gg 1$.

From the above discussion it is obvious that the electric intensity factors at the crack tip are strongly dependent on the boundary condition at the crack surface. In some cases the discontinuous electric spark occurs in the air gap near the crack tip, so the electric intensity factor varies between Cases 2 and 1 or 3. This phenomenon may be related to the electric fatigue damage.

To reveal the structure of the electric field ahead of the crack tip, we consider two special poling directions for a transversely piezoelectric material with its poling axis aligned with the x_2- and the x_1-axis respectively.

4.1. Crack tip fields when the poling direction is aligned with the x_2-axis

When the poling direction is aligned with the x_2-axis, we have

$$\mathbf{H} = 2\begin{pmatrix} 1/C_{\mathrm{L}} & 0 & 0 \\ 0 & 1/C_{\mathrm{T}} & 1/e \\ 0 & 1/e & -1/\varepsilon \end{pmatrix}, \quad \mathrm{Im}[\mathbf{Y}] = \begin{pmatrix} 0 & \psi & -\zeta \\ -\psi & 0 & 0 \\ \zeta & 0 & 0 \end{pmatrix}, \tag{75}$$

where C_{L}, C_{T}, e, ε, ψ, and ζ are some positive material constants for stable materials (see Lothe and Barnett (1976), Suo et al. (1992) and Ru (1999c)). The dimensions of components in Y are given in Suo et al. (1992), and $1/C_{\mathrm{L}}$, $1/C_{\mathrm{T}}$, ψ have the dimensions of [elasticity]$^{-1}$, i.e. m^2/N, $1/e$, ζ have the dimension of [piezoelectricity]$^{-1}$, i.e. m^2/C, and ε has the dimension of permittivity F/m. Here, we adopt the convention by Ru (1999c), which the third column and the third row of the matrices have been deleted and the subscripts used for these 3×3 matrices are 1, 2 and 4. From Eqs. (68), (69), (75), we have

$$D_2(x) = \frac{\varepsilon\sigma_{22}^{\infty}x}{e}\left(\frac{1}{\sqrt{x^2-a^2}} - \frac{1}{\sqrt{x^2-b^2}}\right) + D_2^{\infty}\frac{x}{\sqrt{x^2-b^2}}, \tag{76}$$

$$E_1(x) = \frac{x^2 - I_2/I_1}{\sqrt{x^2-a^2}\sqrt{x^2-b^2}}\frac{\beta_{24}}{2\varepsilon} - \zeta\frac{\sigma_{21}^{\infty}x}{\sqrt{x^2-a^2}}. \tag{77}$$

For a PZT-4 material whose material constants and the electro-mechanical loading relations are listed in the Appendix B, the numerical forms of the above two equations are

$$D_2(x) = \frac{x}{\sqrt{x^2-b^2}}\left(10.03E_2^{\infty} - 0.178\sigma_{11}^{\infty}\right)\times 10^{-9} + \sigma_{22}^{\infty}x\left(\frac{25.33}{\sqrt{x^2-a^2}} - \frac{1.353}{\sqrt{x^2-b^2}}\right)\times 10^{-11}, \tag{78}$$

$$E_1(x) = \frac{x^2 - I_2/I_1}{\sqrt{x^2-a^2}\sqrt{x^2-b^2}}\left(0.0188\sigma_{21}^{\infty} + E_1^{\infty}\right) - 0.0188\frac{\sigma_{21}^{\infty}x}{\sqrt{x^2-a^2}}. \tag{79}$$

Letting $b = 0$ and a, the values for I_2/I_1 are 0 and a^2 respectively, so the crack tip electric field and electric displacement can recovered for the completely conducting and impermeable crack. From Eq. (79), we can see that σ_{21}^{∞} can induce a singular electric field E_1 ahead of the crack tip but σ_{22}^{∞} cannot do.

To show the near-tip electric field and electric displacement variations with respect to the ratio b/a, we consider the electric field and electric displacement at the point $x/a = 1 + (r/a) = 1 + 10^{-5}$, $y = 0$ under the following two loading conditions: (a) only $\sigma_{22}^{\infty} = 1$ MPa, $E_1^{\infty} = 0.1$ MV/m are applied and (b) only $\sigma_{22}^{\infty} = 1$ MPa, $E_2^{\infty} = 0.1$ MV/m are applied. For clarity, we define some normalized quantities appeared in the Figs. 2–5, $\widetilde{D}_{2j} = \sqrt{2\pi r}D_2(a+r,0)/(\sqrt{\pi a}\kappa_{11}E_j^{\infty})$, $\widetilde{E}_{1j} = \sqrt{2\pi r}E_1(a+r,0)/(\sqrt{\pi a}E_j^{\infty})$, $\widetilde{K}_{\mathrm{D}j} = K_{\mathrm{D}}/(\sqrt{\pi a}\kappa_{11}E_j^{\infty})$ and $\widetilde{K}_{\mathrm{E}j} = K_{\mathrm{E}}/(\sqrt{\pi a}E_j^{\infty})$ where j indicates the corresponding remote electric loading and K_{D} and K_{E} are defined by Eqs. (71) and (72) respectively. Figs. 2(a), (b) and 3 give the variations of $\widetilde{D}_{21}$, $\widetilde{E}_{11}$ and $\widetilde{D}_{22}$ with respect to b/a respectively. For a completely impermeable or a completely conducting crack, these values are the corresponding normalized intensity factors. However, in the present model, they are associated to the ratio b/a. For loading condition (b), $E_1(x,0)$ in front of the crack is identically vanishing and it will not be plotted.

It can be seen that $\widetilde{K}_{\mathrm{D}j}$ is almost equal to $\widetilde{D}_{2j}$ for b/a ranging from 0 to 0.9 (Figs. 2(a) and 3). Deviations are observed in the interval for b/a ranging from 0.9 to 1 where the singular fields at $(x = a, 0)$ and $(x = b, 0)$ interacting with each other. The plots for $\widetilde{E}_{11}$ and $\widetilde{K}_{\mathrm{E}1}$ are indiscernible (Fig. 2(b)). This is because the first term in Eq. (77) transits gradually to the impermeable case, not as sharply as the case for $D_2(x,0)$. So the approximation formula of Eq. (72) is exact for most b/a. This conclusion also holds when the poling axis is aligned with the x_1-axis discussed in Section 4.2.

4.2. Crack tip fields when the poling direction is aligned with the x_1-axis

When the poling direction aligned with the x_1-axis, the **H** and Im[**Y**] matrices are

$$\mathbf{H} = 2\begin{pmatrix} 1/C_{\mathrm{T}} & 0 & 1/e \\ 0 & 1/C_{\mathrm{L}} & 0 \\ 1/e & 0 & -1/\varepsilon \end{pmatrix}, \quad \mathrm{Im}[\mathbf{Y}] = \begin{pmatrix} 0 & \psi & 0 \\ -\psi & 0 & \zeta \\ 0 & -\zeta & 0 \end{pmatrix}. \tag{80}$$

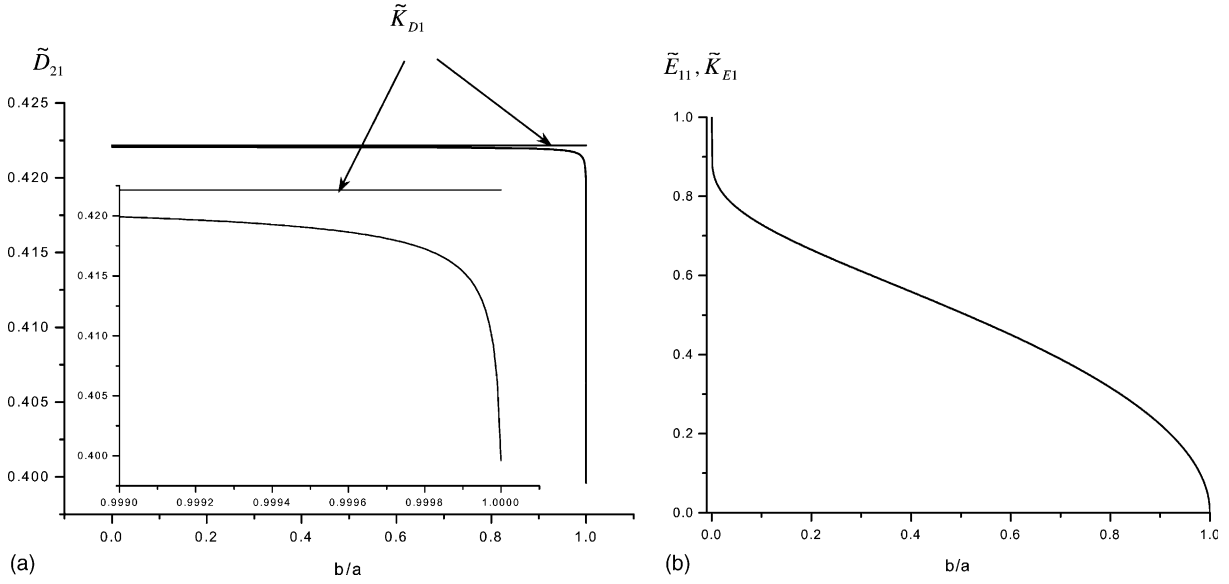

Fig. 2. For the remote loading $\sigma_{22}^{\infty} = 1$ MPa, $E_1^{\infty} = 0.1$ MV/m and x_2 being the poling axis, (a) variations of the $\widetilde{K}_{\mathrm{D}1}$ and $\widetilde{D}_{21}$ with respect to b/a; (b) variations of the $\widetilde{K}_{\mathrm{E}1}$ and $\widetilde{E}_{11}$ with respect to b/a.

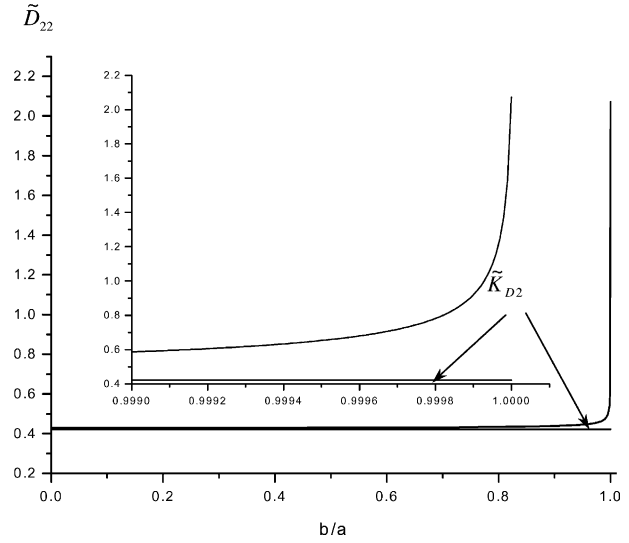

Fig. 3. For the remote loading $\sigma_{22}^{\infty} = 1$ MPa, $E_2^{\infty} = 0.1$ MV/m and x_2 being the poling axis, variations of the $\widetilde{K}_{D_2}$ and $\widetilde{D}_{22}$ with respect to b/a.

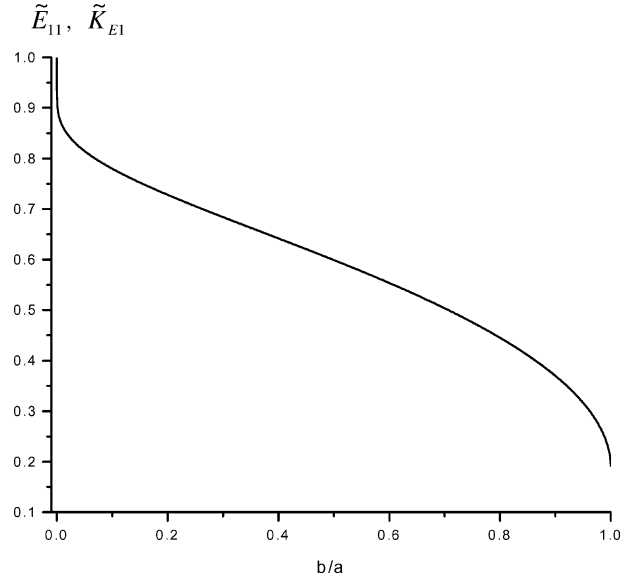

Fig. 4. For the remote loading $\sigma_{22}^{\infty} = 1$ MPa, $E_1^{\infty} = 0.1$ MV/m and x_1 being the poling axis, variations of the $\widetilde{K}_{E_1}$ and $\widetilde{E}_{11}$ with respect to b/a.

So

$$D_2(x) = \frac{\varepsilon \sigma_{22}^{\infty} x}{e}\left(\frac{1}{\sqrt{x^2 - a^2}} - \frac{1}{\sqrt{x^2 - b^2}}\right) + D_2^{\infty}\frac{x}{\sqrt{x^2 - b^2}}, \tag{81}$$

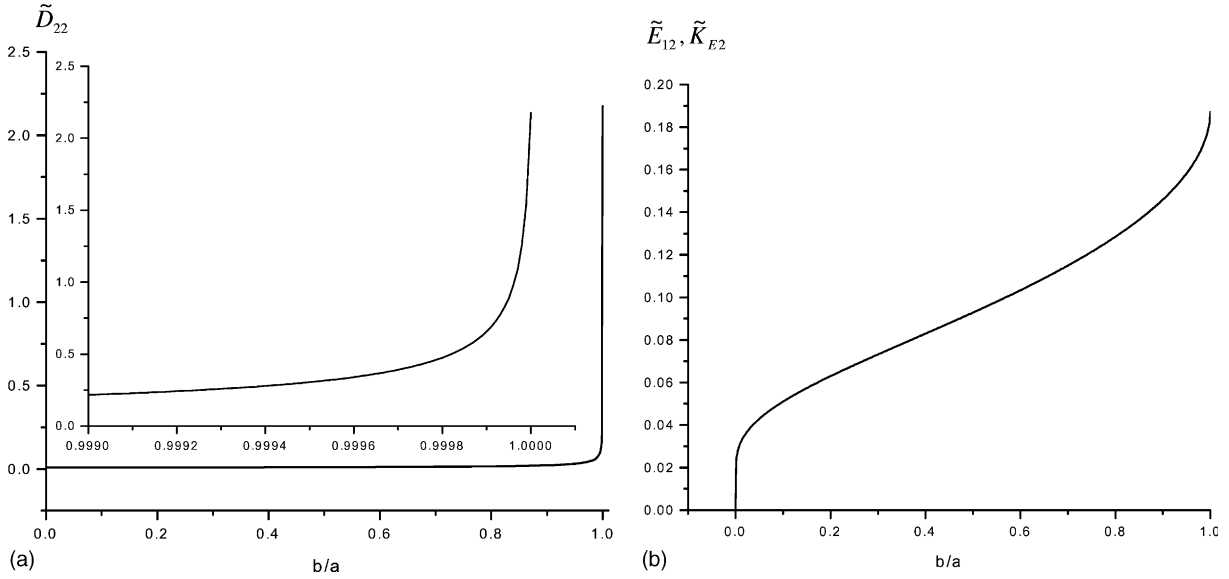

Fig. 5. For the remote loading $\sigma_{22}^{\infty} = 1$ MPa, $E_2^{\infty} = 0.1$ MV/m and x_1 being the poling axis, (a) variations of the $\tilde{D}_{22}$ with respect to b/a ($\tilde{K}_{D_2} = 0$); (b) variations of the $\tilde{K}_{E_2}$ and $\tilde{E}_{12}$ with respect to b/a.

$$E_1(x) = \frac{x^2 - I_2/I_1}{\sqrt{x^2 - a^2}\sqrt{x^2 - b^2}} \left(\frac{\beta_{24}}{2\varepsilon} - \frac{\beta_{21}}{2e} \right) + \zeta \frac{\sigma_{22}^{\infty} x}{\sqrt{x^2 - a^2}}. \tag{82}$$

The numerical expressions of Eqs. (81) and (82) for PZT-4 are as follows:

$$D_2(x) = x \left(\frac{13.056 E_2^{\infty} + 0.2717 \sigma_{21}^{\infty}}{\sqrt{x^2 - b^2}} + \frac{0.2533 \sigma_{21}^{\infty}}{\sqrt{x^2 - a^2}} \right) \times 10^{-9}, \tag{83}$$

$$E_1(x) = \frac{x^2 - I_2/I_1}{\sqrt{x^2 - a^2}\sqrt{x^2 - b^2}} (E_1^{\infty} - 0.0188 \sigma_{22}^{\infty}) + 0.0188 \frac{\sigma_{22}^{\infty} x}{\sqrt{x^2 - a^2}}. \tag{84}$$

Eqs. (83) and (84) can also restore the conducting and impermeable crack tip fields when $b = 0$ and a respectively as in Section 4.1. Eq. (83) manifests that when the poling axis is along x_1, σ_{22}^{∞} can induce a singular electric field E_1 ahead of the crack tip but σ_{21}^{∞} cannot do.

For σ_{22}^{∞} and E_1^{∞} loading, $D_2(x, 0)$ is identically vanishing ahead of the crack tip (Eq. (83)) and will not be plotted. From Fig. 4, $E_1(x, 0)$ decreases as b/a increases from zero to unit. For σ_{22}^{∞} and E_2^{∞}, $E_1(x, 0)$ and $D_2(x, 0)$ both increase as the impermeable length becomes longer (Fig. 5).

Conclusions for the above two subsections are made as follows. The electric field and electric displacement ahead of the crack tip transit from the standard conducting crack to the impermeable crack as b/a changes from zero to unit; for E_1^{∞} loading, making the conducting length shorter is helpful to diminish the electric field and electric displacement concentration near the crack tip irrespective of the poling direction; for E_2^{∞} loading, the longer the conducting length, the smaller the electric field and electric displacement concentration near the crack tip.

5. Energy release rate and the J-integral

It is well known that the crack extension force G is equal to the J-integral

$$J = \int_{\Gamma} (wn_1 - n_i\sigma_{ip}u_{p,1} - n_iD_i\phi_{,1})\,\mathrm{d}s \tag{85}$$

when the contour Γ only surrounds the crack tip and the crack faces are free of external charge and traction (Pak, 1990; Suo et al., 1992). In Eq. (85) w is electric enthalpy. In the present model, the numerical computation for J-integral will also be classified as that stated in Section 4 for crack tip fields. First, we give the crack tip ERR by the Irwin closure integral (Suo, 1993)

$$G = \lim_{l\to 0} \frac{1}{2l} \int_0^l \left\{\sigma_{2j}(l-r,0)\left[u_j(r,\pi) - u_j(r,-\pi)\right] + E_1(l-r,0)[q(r,\pi) - q(r,-\pi),]\right\}\mathrm{d}r, \tag{86}$$

where q is the electric charge accumulated on the conducting crack surfaces and l is an infinitesimal crack extension length. Note that Eq. (86) holds only under the assumption that r is much smaller than the length δ. Hence, we have

$$G = \frac{\pi\sigma_{2j}^{\infty}\sigma_{2k}^{\infty}a}{4}\left[H_{jk} - \frac{H_{j4}H_{4k}}{H_{44}}\right] - \frac{\pi(I_2/I_1 - a^2)^2}{4a(a^2-b^2)}\frac{(H_{4K}\beta_{2K})^2}{H_{44}}. \tag{87}$$

We define the J-integral as J^{I} when Γ surrounds only the right crack tip ($x = a$) and J^{II} when Γ surrounds two singular points ($x = a, 0$) and ($x = b, 0$) (Fig. 6). Our numerical results find that G is always identical to J^{I} as shown by theoretical analysis. Eq. (87) can be reduced to the completely conducting crack solution, but it cannot to the completely impermeable crack solution when $b = a$. The reason is that: when the crack becomes completely impermeable, two singular points $x = a$ and $x = b$ coincide with each other, but the ERR defined by Eq. (86), which is equal to J^{I}, does not include the singularity at $x = b$. To evaluate the correct ERR for an impermeable crack, the contour Γ must contain two singularities, and our numerical and theoretical results find that the ERR obtained from completely impermeable crack (Suo et al., 1992) for an impermeable crack is definitely equal to J^{II}. In order to study this phenomenon further, we show both the variations of J^{I} and J^{II} with respect to the ratio b/a. So in the numerical calculation, the half crack

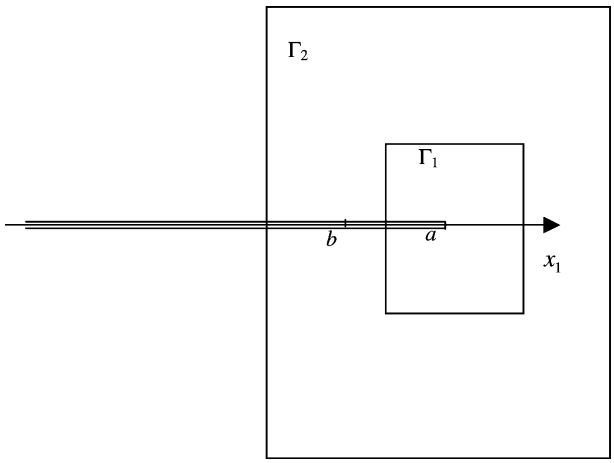

Fig. 6. Illustration of the two integral contours Γ_1 and Γ_2 surrounding one singularity and two singularities respectively.

Table 1
Table for the ERR for the completely insulating and conducting cracks with the half crack length $a = 0.1$ m

Loading condition	$\sigma_{22}^{\infty} = 1$ MPa; $E_1^{\infty} = 0.1$ MV/m	$\sigma_{22}^{\infty} = 1$ MPa; $E_2^{\infty} = 0.1$ MV/m	$\sigma_{22}^{\infty} = 1$ MPa for references
Conducting (poling axis x_1)	14.61	3.402	3.402
Insulating (poling axis x_1)	2.767	−20.64	2.767
Conducting (poling axis x_2)	21.595	3.629	3.629
Insulating (poling axis x_2)	3.626	−9.826	3.626

The unit for ERR is N/m.

length a is assumed to be 0.1 m. Table 1 shows the ERR for the completely conducting and impermeable cracks for three loading conditions for comparison with the plots of J^{I} and J^{II}.

Figs. 7–10 give the plots of the variations of J^{I} and J^{II} with respect to the ratio b/a. From Figs. 7(a), 9(a) and 10(a), it is revealed that J^{I} decreases as b/a increasing (i.e. the conducting length decreasing). Fig. 8(a) shows that under this loading condition, J^{I} is irrespective of the ratio b/a. The ERR for a completely conducting crack can be obtained from J^{I} (Figs. 7(a)–10(a)) and the ERR for a completely impermeable crack can be obtained from J^{II} as shown in Figs. 7(b)–10(b) when b/a approaches to unit. These figures also show that the difference between J^{I} and J^{II} is obvious. For $b/a > 0.9$, we see in Figs. 8(b) and 10(b), when E_2^{∞} is applied J^{II} decreases with increasing b/a, but Figs. 7(b) and 9(b) show that when E_1^{∞} is applied b/a is no influence on J^{II}. This means that as the impermeable length increases the impermeable singularity at $x = b$ comes into effect. It can be concluded from Figs. 7–10 that as the impermeable length increases the ERR decreases. It is also noted that for classical conducting crack $J = G > 0$ and in our case J is the lower limit of J^{I}, so always $J^{\mathrm{I}} > 0$. For classical insulating crack J may be negative and in our case J is the upper limit of J^{II}, so J^{II} may be positive or negative. In practical experiments the crack tip condition is very important. If the air gap behind the insulation crack tip is breakdown then the J value increases and may give rise to damage. The spark phenomenon may lead to fatigue.

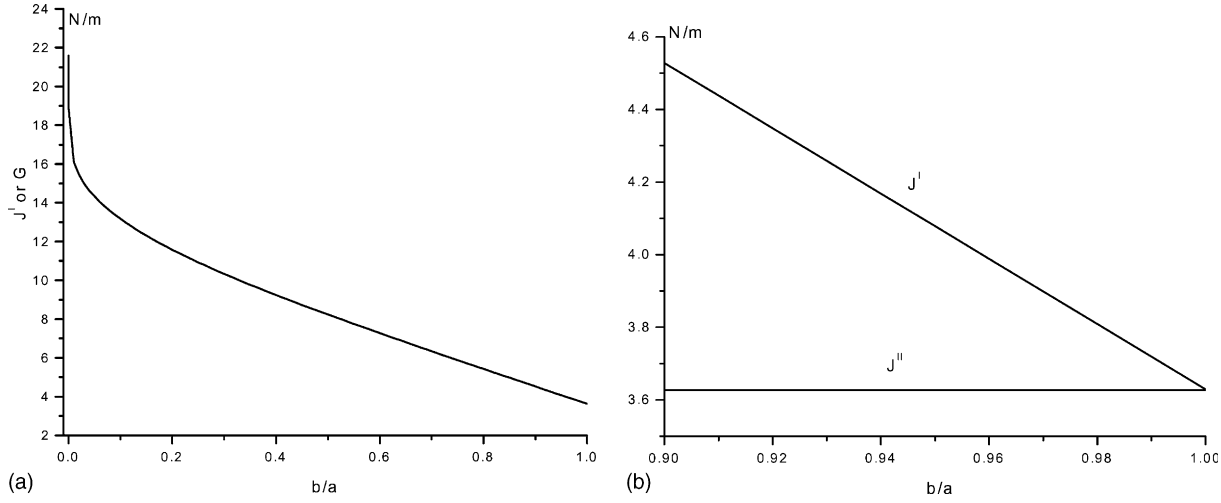

Fig. 7. Variations of J-integral value with respect to b/a under the loading $\sigma_{22}^{\infty} = 1$ MPa, $E_1^{\infty} = 0.1$ MV/m for the poling axis aligned with x_2-axis (a) J^{I}; (b) J^{I} and J^{II}.

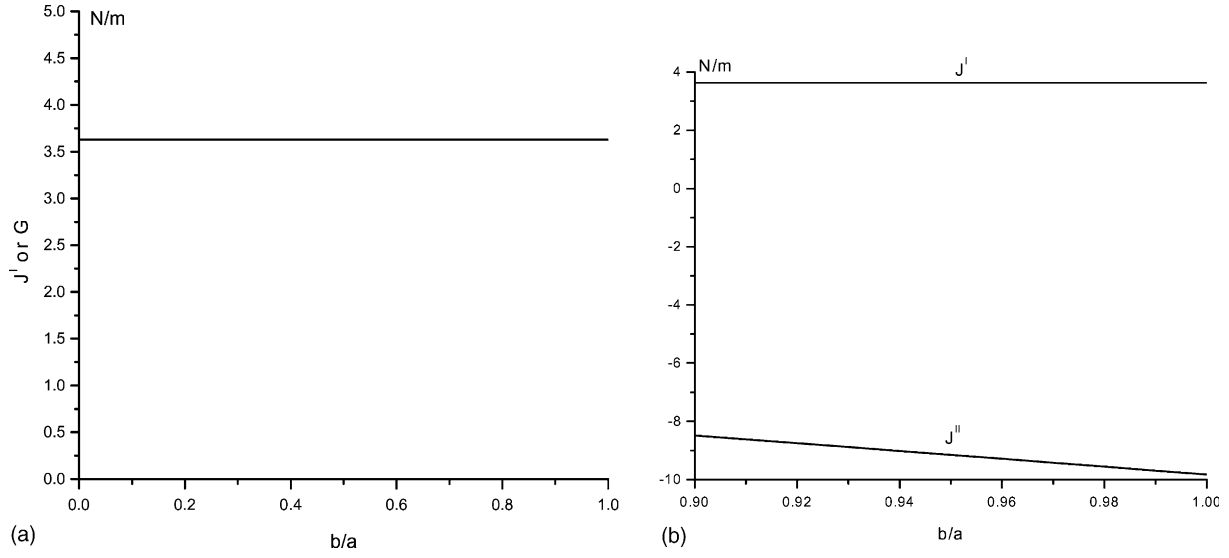

Fig. 8. Variations of J-integral value with respect to b/a under the loading $\sigma_{22}^{\infty} = 1$ MPa, $E_2^{\infty} = 0.1$ MV/m for the poling axis aligned with x_2-axis (a) J^{I}; (b) J^{I} and J^{II}.

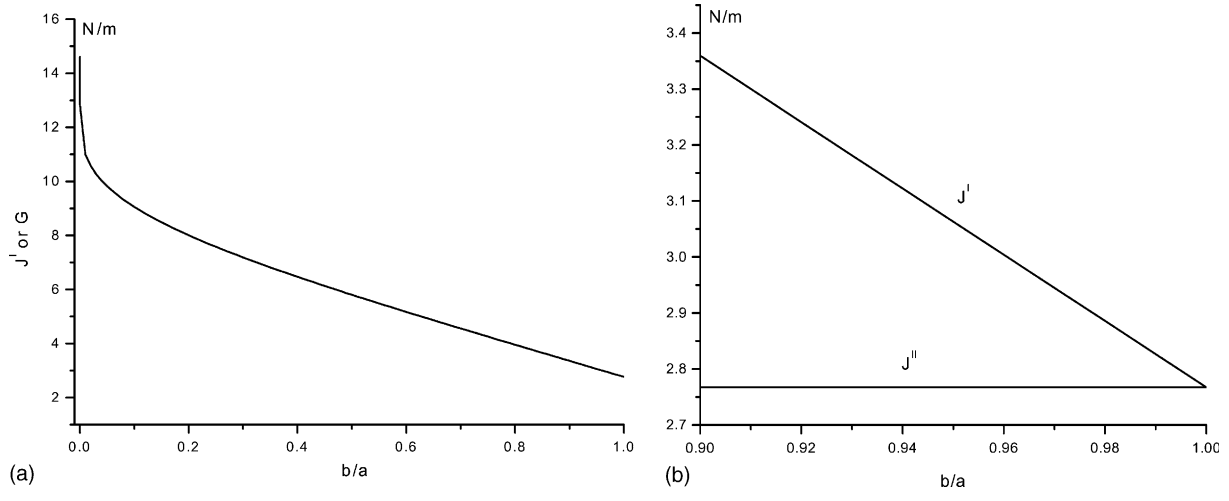

Fig. 9. Variations of J-integral value with respect to b/a under the loading $\sigma_{22}^{\infty} = 1$ MPa, $E_1^{\infty} = 0.1$ MV/m for the poling axis aligned with x_1-axis (a) J^{I}; (b) J^{I} and J^{II}.

Experiments show that crack extension is determined by the stress state within a characteristic distance r_0 ahead of the crack tip, so when $\delta \gg r_0$, then J^{I} is an appropriate control parameter for fracture, but J^{II} is an appropriate one for $\delta \ll r_0$. This conclusion is consistent with the near-tip electric fields and electric displacement fields analysis in Section 4. This proposition is also consistent with Kuang's opinion (Kuang and Mao, 1996; Kuang and Ma, 2002) about the maximum ERR criterion. That opinion indicated that the

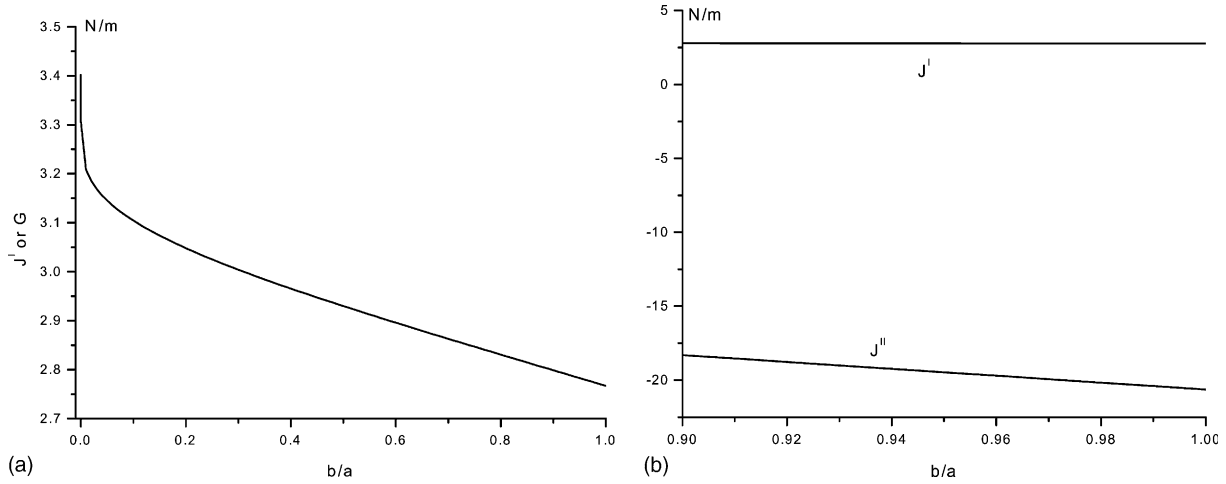

Fig. 10. Variations of J-integral value with respect to b/a under the loading $\sigma_{22}^{\infty} = 1$ MPa, $E_2^{\infty} = 0.1$ MV/m for the poling axis aligned with x_1-axis (a) J^{I}; (b) J^{I} and J^{II}.

direction of crack extension should be determined by the singular field at the main crack tip before extension, and that applying the J-integral only around the branched crack tip is not appropriate.

6. Conclusions

In this paper, using the Stroh formalism, a mixed electric boundary value problem for a two-dimensional piezoelectric crack problem is solved. The results suggest that the stress intensity factors are identical to those of conventional impermeable or conducting cracks. The electric field and electric displacement exhibit singularity at crack tips but also at the junctures between the impermeable parts and conducting parts. The electric field ahead of the crack tip transits from the standard conducting crack to the impermeable crack as b/a changes from zero to unit. For E_1^{∞} loading, increasing b/a is helpful to diminish the electric field and electric displacement concentration near the crack tip irrespective of the poling direction; for E_2^{∞} loading, the longer the conducting length, the smaller the electric field and electric displacement concentration near the crack tip. The research about J-integral shows that when the distance between two singular points is less than the fracture characteristic length, J^{II} is an appropriate control parameter for fracture, otherwise, $\delta \gg r_0$, J^{I} is an appropriate one. As a first step for future study of the complicated electric boundary problem involved in the experiment, the model proposed in the present paper still awaits experimental tests and needs further investigation to meet the experimental situation more precisely.

Acknowledgements

This work is supported by the national science foundation of China through the grant 10072033 and the grant 10132010.

Appendix A. Some definite integrals

$$\begin{cases} \displaystyle\int_L \frac{X_{ab}^+(t)}{t-z}\,\mathrm{d}t = \int_{L_1\cup L_3} \frac{X_{ab}^+(t)}{t-z}\,\mathrm{d}t = \pi i X_{ab}(z), \\ \displaystyle\int_L \frac{X_{ab}^+(t)}{t-x}\,\mathrm{d}t = \int_{L_1\cup L_3} \frac{X_{ab}^+(t)}{t-x}\,\mathrm{d}t = 0, & x\in L_1\cup L_3, \\ \displaystyle\int_L \frac{X_{ab}^+(t)}{t-x}\,\mathrm{d}t = \int_{L_1\cup L_3} \frac{X_{ab}^+(t)}{t-x}\,\mathrm{d}t = \pi i X_{ab}^+(x), & x\in L_2. \end{cases}$$

$$\begin{cases} \displaystyle\int_L \frac{tX_{ab}^+(t)}{t-z}\,\mathrm{d}t = \int_{L_1\cup L_3} \frac{tX_{ab}^+(t)}{t-z}\,\mathrm{d}t = \pi i z X_{ab}(z), \\ \displaystyle\int_L \frac{tX_{ab}^+(t)}{t-x}\,\mathrm{d}t = \int_{L_1\cup L_3} \frac{tX_{ab}^+(t)}{t-x}\,\mathrm{d}t = 0, & x\in L_1\cup L_3, \\ \displaystyle\int_L \frac{tX_{ab}^+(t)}{t-x}\,\mathrm{d}t = \int_{L_1\cup L_3} \frac{tX_{ab}^+(t)}{t-x}\,\mathrm{d}t = \pi i x X_{ab}^+(x), & x\in L_2. \end{cases}$$

$$\begin{cases} \displaystyle\int_L \frac{t^2X_{ab}^+(t)}{t-z}\,\mathrm{d}t = \int_{L_1\cup L_3} \frac{t^2X_{ab}^+(t)}{t-z}\,\mathrm{d}t = \pi i (z^2 X_{ab}(z)-1), \\ \displaystyle\int_L \frac{t^2X_{ab}^+(t)}{t-x}\,\mathrm{d}t = \int_{L_1\cup L_3} \frac{t^2X_{ab}^+(t)}{t-x}\,\mathrm{d}t = -\pi i, & x\in L_1\cup L_3, \\ \displaystyle\int_L \frac{t^2X_{ab}^+(t)}{t-x}\,\mathrm{d}t = \int_{L_1\cup L_3} \frac{t^2X_{ab}^+(t)}{t-x}\,\mathrm{d}t = \pi i (x^2 X_{ab}^+(x)-1), & x\in L_2. \end{cases}$$

$$\begin{cases} \displaystyle\int_L \frac{X_b^+(t)}{(t-z)X_a^+(t)}\,\mathrm{d}t = \int_{L_1\cup L_3} \frac{X_b^+(t)}{(t-z)X_a^+(t)}\,\mathrm{d}t = \pi i\left(\frac{X_b(z)}{X_a(z)}-1\right), \\ \displaystyle\int_L \frac{X_b^+(t)}{(t-x)X_a^+(t)}\,\mathrm{d}t = \int_{L_1\cup L_3} \frac{X_b^+(t)}{(t-x)X_a^+(t)}\,\mathrm{d}t = -\pi i, & x\in L_1\cup L_3, \\ \displaystyle\int_L \frac{X_b^+(t)}{(t-x)X_a^+(t)}\,\mathrm{d}t = \int_{L_1\cup L_3} \frac{X_b^+(t)}{(t-x)X_a^+(t)}\,\mathrm{d}t = \pi i\left(\frac{X_b^+(x)}{X_a^+(x)}-1\right), & x\in L_2. \end{cases}$$

$$\begin{cases} \displaystyle\int_L \frac{tX_b^+(t)}{(t-z)X_a^+(t)}\,\mathrm{d}t = \int_{L_1\cup L_3} \frac{tX_b^+(t)}{(t-z)X_a^+(t)}\,\mathrm{d}t = \pi i z (X_b(z)/X_a(z)-1), \\ \displaystyle\int_L \frac{tX_b^+(t)}{(t-x)X_a^+(t)}\,\mathrm{d}t = \int_{L_1\cup L_3} \frac{tX_b^+(t)}{(t-x)X_a^+(t)}\,\mathrm{d}t = -\pi i x, & x\in L_1\cup L_3, \\ \displaystyle\int_L \frac{tX_b^+(t)}{(t-x)X_a^+(t)}\,\mathrm{d}t = \int_{L_1\cup L_3} \frac{tX_b^+(t)}{(t-x)X_a^+(t)}\,\mathrm{d}t = -\pi i x, & x\in L_2. \end{cases}$$

Appendix B. Material constants and remote electro-mechanical loading relations

The material constants for PZT-4 whose poling axis is along x_3-axis are listed as follows (Park and Sun, 1995):

$$c_{11} = 139, \quad c_{33} = 113, \quad c_{12} = 77.8, \quad c_{13} = 74.3, \quad c_{44} = 25.6 \text{ (GPa)},$$
$$e_{33} = 13.8, \quad e_{31} = -6.98, \quad e_{15} = 13.4 \text{ (Cm}^{-2}\text{)},$$
$$\kappa_{11} = 6.00 \times 10^{-9}, \quad \kappa_{33} = 5.47 \times 10^{-9} \text{ (C}^2\text{N}^{-1}\text{m}^{-2}\text{)}.$$

The numerical forms of the matrix **H** and Im[**Y**] in Eq. (75) are:

$$C_L = 5.68 \times 10^{10} \text{ N/m}^2, \quad C_T = 5.72 \times 10^{10} \text{ N/m}^2, \quad \psi = 7.62 \times 10^{-12} \text{ N/m}^2,$$
$$e = 45.15 \text{ C/m}^2, \quad \zeta = 1.88 \times 10^{-2} \text{ C/m}^2, \quad \varepsilon = -5.72 \times 10^{-9} \text{ F/m}.$$

In practice an application of remote electric displacement loading is more difficult than an application of electric field, so in this paper we express all quantities in terms of E_i^∞ instead of D_i^∞. When the poling axis is directed along the x_2-axis, the relation between the remote electric displacement and the electric field are:

$$\begin{aligned} D_1^\infty &= 1.306 \times 10^{-8} E_1^\infty + 5.25 \times 10^{-10} \sigma_{12}^\infty \text{ (C/m}^2\text{)}, \\ D_2^\infty &= 1.003 \times 10^{-8} E_2^\infty - 1.783 \times 10^{-10} \sigma_{11}^\infty + 2.398 \times 10^{-10} \sigma_{22}^\infty \text{ (C/m}^2\text{)}. \end{aligned} \tag{B.1}$$

The relation between the remote electric displacement and the electric field for the poling direction along the x_1-axis are

$$\begin{aligned} D_1^\infty &= 1.003 \times 10^{-8} E_2^\infty - 1.783 \times 10^{-10} \sigma_{11}^\infty + 2.398 \times 10^{-10} \sigma_{22}^\infty \text{ (C/m}^2\text{)}, \\ D_2^\infty &= 1.306 \times 10^{-8} E_1^\infty + 5.25 \times 10^{-10} \sigma_{12}^\infty \text{ (C/m}^2\text{)}, \end{aligned} \tag{B.2}$$

which can be obtained by a coordinate transformation rule.

Appendix C. The reasonableness of the impermeable conditions on the boundary of the elliptic cavity

According to Gao and Fan (1999); Kuang and Ma (2002), the exact solution of a transversely isotropic cavity filled air is

$$F_\alpha(z_\alpha) = C_\alpha + (\beta_{\alpha 1} l_1 + \beta_{\alpha 2} l_2 + \beta_{\alpha 3} l_3) \frac{1}{a + i p_\alpha b} \left[1 - \frac{z_\alpha}{\sqrt{z_\alpha^2 - (a^2 + p_\alpha^2 b^2)}} \right],$$

where C_α is the function of σ_{ij}^∞ and p_α, l_1 and l_2 are functions of σ_{ij}^∞ and the sizes of ellipse, $\beta_{\alpha\gamma}$ is the function of p_α and material constants. Their expressions can be found in Gao and Fan (1999) and Kuang and Ma (2002), and are omitted here. Only l_3 is related to electric displacements D_1^c and D_2^c in the elliptic cavity with air and its expression is

$$l_3 = \frac{1}{2} [a(D_2^\infty - D_2^c) - ib(D_1^\infty - D_1^c)].$$

Due to the permittivity ε_0 of air is very small compared to that of the dielectric, so $D_2^\infty - D_2^c \approx D_2^\infty$, $D_1^\infty - D_1^c \approx D_1^\infty$. If $D_2^\infty = D_1^\infty = 0$, then l_3 is very small compared with l_1 and l_2. Therefore, the exact jointed conditions at the boundary of ellipse filled with air can be approximated by an impermeable boundary condition.

References

Chung, M.Y., Ting, T.C.T., 1996. Piezoelectric solid with an elliptic inclusion or hole. International Journal of Solids and Structures 33, 3343–3461.

Deeg, W.F., 1980. The analysis of dislocation, crack and inclusion problems in piezoelectric solids. Ph.D. thesis, Stanford University, CA.

Fu, R., Zhang, T.-Y., 1998. Effects of an applied electric field on the modulus of rupture of poled lead Zirconate Titanate Ceramics. Journal of American Ceramic Society 81, 1058–1060.
Fu, R., Zhang, T.-Y., 2000. Effects of an electric field on the fracture toughness of poled lead Zirconate Titanate Ceramics. Journal of American Ceramic Society 83, 1215–1218.
Fulton, C.C., Gao, H., 1997. Electrical non-linearity in fracture of piezoelectric ceramics. ASME Applied Mechanics Review 50, S56–S63.
Gao, C.-F., Fan, W.-X., 1999. Exact solutions for the plane problem in piezoelectric materials with an elliptic or a crack. International Journal of Solids and Structures 36, 2527–2540.
Gao, H., Zhang, T.-Y., Tong, P., 1997. Local and global energy release rates for an electrically yielded crack in a piezoelectric ceramic. Journal of the Mechanics and Physics of Solids 45, 491–510.
Gradshteyn, I.S., Ryzhik, I.M., 1980. Table of Integrals, Series, and Products. Academic Press, New York.
Huang, Z., Kuang, Z.-B., 2000. Asymptotic electro-elastic field near a blunt crack tip in a transversely isotropic piezoelectric material. Mechanics Research Communications 27, 601–606.
Huang, Z., Kuang, Z.-B., 2001. A first order perturbation analysis of a non-ideal crack in a piezoelectric material. International Journal of Solids and Structures 38, 7261–7281.
Jiang, L.Z., Sun, C.T., 2001. Analysis of indentation cracking in piezoceramics. International Journal of Solids and Structures 38, 1903–1918.
Kuang, Z.-B., 1982. The stress field near the blunt crack tip and the fracture criterion. Engineering Fracture Mechanics 16, 19–33.
Kuang, Z.-B., Ma, F.-S., 2002. The Crack Tip Fields. Xi'an Jiaotong University publishing house, Xi'an.
Kuang, Z.-B., Mao, Y.-J., 1996. A note on the stress analysis of a branched crack under the longitudinal shear. In: Yu, S.-W. et al. (Eds.), Advances of Solid Mechanics. Tsinghua University Press, Beijing.
Lothe, J., Barnett, D.M., 1976. Integral formalism for surface waves in piezoelectric crystals. Existence considerations. Journal of Applied Physics 47, 1799–1807.
Lynch, C.L., 1998. Fracture of ferroelectric and relaxor electric-ceramics: influence of electric field. Acta Materialia 46, 599–608.
Lynch, C.S., Chen, L., Suo, Z., McMeeking, R.M., 1995a. Crack growth in ferroelectric ceramics driven by cyclic polarization switching. Journal of Intelligent Material Systems and Structures 6, 191–198.
Lynch, C.S., Yang, W., Collier, L., Suo, Z., McMeeking, R.M., 1995b. Electric field induced cracking in ferroelectric ceramics. Ferroelectrics 166, 11–30.
Muskhelishvili, N.I., 1953. Some Basic Problems of the Mathematical Theory of Elasticity. Noordhoff, Leyden.
Pak, Y.E., 1990. Crack extension force in a piezoelectric material. ASME Journal of Applied Mechanics 57, 647–653.
Pak, Y.E., 1992. Linear electro-elastic fracture mechanics of piezoelectric materials. International Journal of Fracture 54, 79–100.
Park, S., Sun, C.T., 1995. Fracture criteria for piezoelectric materials. Journal of American Ceramic Society 78, 1475–1480.
Parton, V.Z., 1976. Fracture mechanics of piezoelectric materials. Acta Astronautica 3, 671–683.
Ru, C.Q., 1999a. Conducting cracks in a piezoelectric ceramic of limited electrical polarization. Journal of the Mechanics and Physics of Solids 47, 2125–2146.
Ru, C.Q., 1999b. Effect of electric polarization saturation on stress intensity factors in a piezoelectric ceramics. International Journal of Solids and Structures 36, 869–883.
Ru, C.Q., 1999c. Electric-field induced crack closure in linear piezoelectric media. Acta Materialia 47, 683–693.
Sosa, H.A., Khutoryansky, N., 1996. New developments concerning piezoelectric materials with defects. International Journal of Solids and Structures 33, 3399–3414.
Suo, Z., 1993. Models for breakdown-resistant dielectric and ferroelectric ceramics. Journal of the Mechanics and Physics of Solids 41, 1155–1176.
Suo, Z., Kuo, C.M., Barnett, D.M., Willis, J.R., 1992. Fracture mechanics for piezoelectric ceramics. Journal of the Mechanics and Physics of Solids 40, 739–765.
Ting, T.C.T., 1996. Anisotropic Elasticity and it's Application. Oxford University Press, London.
Wang, H., Singh, R.N., 1997. Crack propagation in piezoelectric ceramics: effects of applied electric fields. Journal of applied physics 81, 7471–7479.
Yang, W., Zhu, T., 1998. Switch toughening of ferroelectrics subjected to electric fields. Journal of the Mechanics and Physics of Solids 46, 291–311.
Zhang, T.-Y., Fu, R., Zhao, M., Tong, P., 2000. Overview of fracture of piezoelectric ceramics. Key Engineering Materials 183, 695–706.
Zhang, T.-Y., Zhao, M., Tong, P., 2001. Fracture of piezoelectric ceramics. Advances in Applied Mechanics 38, 147–289.
Zhu, T., Yang, W., 1997. Toughness variation of ferroelectrics by polarization switch under non-uniform electric field. Acta Materialia 45, 4695–4702.